



## 19 **Abstract**

20 Emulators of Earth System Models (ESMs) are complementary to ESMs by providing climate  
21 information at lower computational costs. Thus far, the emulation of spatially resolved climate  
22 extremes has only received limited attention, even though it is one of the most impactful aspects  
23 of climate change. Here, we propose a method for the emulation of local annual maximum  
24 temperatures, with a focus on reproducing essential statistical properties such as correlations in  
25 space and time. We test different emulator configurations and find that driving the emulations  
26 with global mean surface temperature offers an optimal compromise of model complexity and  
27 performance. We show that the emulations can mimic the temporal evolution and spatial patterns  
28 of the underlying climate model simulations and are able to reproduce their natural variability.  
29 The general design and the good performance for annual maximum temperatures suggests that  
30 the proposed methodology can be applied to other climate extremes.

31

## 32 **Plain Language Summary**

33 Climate models are invaluable tools for studying climate change but take a very long time to run,  
34 even on modern super computers. Emulators of climate models are statistical tools that can be  
35 calibrated to mimic the behaviour of complex climate models with a much reduced  
36 computational demand. However, they are typically not made for reproducing climate extremes,  
37 despite the fact that extreme climate events belong to the most impactful aspects of climate  
38 change. In this study, we propose a method for the emulation of annual maximum temperature  
39 over time and space. This method also reproduces the natural variability of climate models, even  
40 though it is driven only by global mean surface temperature. We show that the emulations are  
41 very similar to the data created by climate models. In an example application, we use the  
42 emulator to examine the extreme temperatures for different climate scenarios.

43

44 **TOTAL WORDS: 3892 / 4000**

45

## 46 **1 Introduction**

47 The impacts of climate change will affect the entire social and economical system (IPCC,  
48 2014, 2021). In particular, changes in climate extremes count among the most impactful  
49 consequences of climate change. Climate extremes are substantially affected by human-induced  
50 climate change (Seneviratne et al., 2021). For example, the annual average losses to weather-  
51 related disasters were USD168 billions per year over 2001-2010 and have increased to USD248  
52 billions per year over 2011-2020 (Aon, 2021). Climate extremes affect numerous economical  
53 sectors, for instance agriculture (Sivakumar et al., 2005; Vogel et al., 2019) or the energy sector  
54 (Schaeffer et al., 2012; Perera et al., 2020). Not only do climate extremes have direct  
55 consequences on food or energy security (Hasegawa et al., 2021), but they may also have  
56 indirect impacts on societies due to feedbacks with societal drivers (Raymond et al., 2020). Even  
57 if climate change is limited to 1.5°C, changes in climate extremes remain a crucial issue  
58 (Seneviratne et al., 2018), and society will be impacted in many aspects (IPCC, 2018).

59 Traditionnaly, Earth System Models (ESMs) are used to derive climate change  
60 projections and the associated climate extremes (Flato et al., 2013; Collins et al., 2013; Lee et al.,

61 2021). These outputs are crucial to assess what consequences climate extremes would have on  
62 society (Rosenzweig et al., 2017). However, ESMs require detailed scenarios to simulate climate  
63 change and have very high computational cost, solving a very large number of equations on  
64 several grids. These requirements make ESMs expensive tools and hinder their use to explore  
65 new scenarios and to characterize the internal climate variability.

66 ESM emulators have been developed for a quicker assessment of climate change in  
67 response to given scenario pathways. A large class of emulators, termed “simple climate models”  
68 or “reduced complexity models” provide projections of key variables of the Earth system such as  
69 global mean temperature (Nicholls et al., 2020; Nicholls et al., 2021), however they do not  
70 provide local information which is essential for studying climate impacts. A second class of  
71 emulators derives spatially resolved climate responses from global mean temperature trajectories  
72 (“spatially resolved emulators”), such as the recently developed Modular Earth System Model  
73 Emulator with spatially Resolved output (MESMER) (Beusch et al., 2020) that this work builds  
74 upon. Spatially resolved emulators usually rely on some version of pattern scaling to derive local  
75 responses from global variables (Mitchell, 2003; Fordham et al., 2012; Herger et al., 2015;  
76 Lynch et al., 2017; Alexeeff et al., 2018). While other approaches exist (Castruccio et al., 2014;  
77 Holden et al., 2014), pattern scaling shows good performances in spite of its simplicity (Tebaldi  
78 and Arblaster, 2014; Tebaldi and Knutti, 2018). For the representation of natural variability,  
79 there is no single most established method. Some emulators resample actual ESM fields  
80 (McKinnon et al., 2017; Alexeeff et al., 2018), some resample principle components with  
81 perturbed phases (Link et al., 2019), and others rely on autoregressive processes with spatially  
82 correlated innovations (Beusch et al., 2020; Nath et al., 2021). Almost all currently available  
83 spatially resolved emulation approaches have been developed to emulate mean quantities, but to  
84 better assess the impacts of climate change for diverse emission pathways, emulation of climate  
85 extremes is needed too. A first step in this direction has been made by (Tebaldi et al., 2020),  
86 using pattern scaling to emulate the average evolution of climate extremes, but does not consider  
87 natural variability. Thus, an emulator that reproduces the full distribution of the climate extremes  
88 is still lacking.

89 In this paper, we propose a new method for the emulation of climate extremes that  
90 accounts for both the spatio-temporal structure and their internal variability. Building on the  
91 MESMER emulator, the presented approach is referred as MESMER-X. The statistical  
92 framework of the method is introduced in Section 3. We use annual maximum temperature data  
93 from the 6<sup>th</sup> phase of the Coupled Model Intercomparison Project (CMIP6, (Eyring et al., 2016))  
94 to illustrate our method (Section 4). Finally, we discuss the potential of this method for extension  
95 to other climate extremes (Section 5).

96

## 97 **2 Data**

98 Simulations from 18 ESMs contributing to Scenario Model Intercomparison Project  
99 (ScenarioMIP, (O'Neill et al., 2016)) of CMIP6 are considered (listed in Supplementary table  
100 S.1). We use the ESMs which provide data for concentration-driven historical (Meinshausen et  
101 al., 2017) and for at least two of the five scenarios SSP1-1.9, SSP1-2.6, SSP2-4.5, SSP3-7.0 and  
102 SSP5-8.5 (Meinshausen et al., 2020). As another condition, we retain only the ESMs providing  
103 the daily maximum near-surface air temperature, the near-surface air temperature and the  
104 downward surface sensible heat flux over the ocean.

105 All simulations are interpolated to the same  $2.5^\circ \times 2.5^\circ$  grid using second-order  
 106 conservative remapping for the two temperatures and inverse distance-weighted average  
 107 remapping for the heat flux (Brunner et al., 2020a). Spatially resolved local annual maximum  
 108 temperature (TXx) is calculated as the annual maximum of the daily maximum temperature. The  
 109 anomaly of the local annual maximum temperature is defined by subtracting the 1850-1900  
 110 mean. The global mean surface air temperature (GSAT) is derived by first averaging annual mean  
 111 near-surface temperature, then its anomaly is also calculated by subtracting the 1850-1900 mean.  
 112 The same operations are performed to obtain the global downward heat flux in sea water  
 113 (HFDS).

114 In Section 4, both the global trend and global variability of GSAT and HFDS are used to  
 115 identify adequate drivers for the emulations. These two components are decomposed using a  
 116 locally weighted scatterplot smoothing, accounting for volcanic eruptions as explained in  
 117 (Beusch et al., 2020). For the sake of clarity, this paper shows mostly results with the global  
 118 trend of GSAT, but the full results are shown in supplementary information.

119 In this paper, some results are aggregated to sub-continental regions defined for the 6<sup>th</sup>  
 120 Assessment Report of IPCC regions (Iturbide et al., 2020).

121

## 122 **3 A method for the emulation of climate extremes**

### 123 3.1 Statistical distribution of local climate extremes

124 Climate variables can be characterized by stochastic processes, and climate extremes are  
 125 rare values or events of these climate variables, in the tail of their probability distribution (Wilks,  
 126 2011; Storch and Zwiers, 1999). This definition implies that changes in the distribution of  
 127 climate variables will also affect the distribution of climate extremes. For instance, if the local  
 128 annual surface temperature increases, it is likely that the local annual maximum surface  
 129 temperature will increase as well. Regional anomalies of climate extremes have been found to  
 130 scale linearly with anomalies in GSAT (Seneviratne et al., 2016; Wartenburger et al., 2017;  
 131 Seneviratne et al., 2018; Tebaldi et al., 2020). Here, the principle is extended: instead of having  
 132 the regional mean anomalies of climate extremes scaled with anomalies in GSAT, we scale the  
 133 distribution of the local anomalies of climate extremes with anomalies in GSAT.

134 For clarity, this method is explained for TXx, but this method is designed to be applicable  
 135 to other climate extremes as discussed in Section 5. We write  $\Delta X_{s,t}$  the local anomaly of TXx at  
 136 each point in space  $s$  and timestep  $t$ . We assume here that  $\Delta X_{s,t}$  follows a Generalized Extreme  
 137 Value (GEV) distribution, because TXx is a block maxima (Coles, 2001; Wilks, 2011) and we  
 138 note that the GEV has been successfully used to model TXx elsewhere (Hauser et al., 2016;  
 139 Huang et al., 2016; Kim et al., 2020). We further assume that the location, scale and shape  
 140 parameters of the GEV are point- and timestep-dependent, written as  $\mu_{s,t}$ ,  $\sigma_{s,t}$  and  $\xi_{s,t}$ . More  
 141 precisely, we disentangle these dependencies by assuming that these parameters follow the  
 142 functions  $f_s$ ,  $g_s$  and  $h_s$ , taking a matrix of covariates  $\Delta \mathbf{V}_t$  as input. This matrix is defined as

143 timeseries of the anomalies in global climate variables such as GSAT. We define the emulator  
 144 configuration  $E$  as the set of equations (1). Examples are shown in Section 4.1.

$$145 \quad E: \begin{cases} \Delta X_{s,t} \sim GEV(\mu_{s,t}, \sigma_{s,t}, \xi_{s,t}) \\ \mu_{s,t} = f_s(\Delta \mathbf{V}_t) \\ \sigma_{s,t} = g_s(\Delta \mathbf{V}_t) \\ \xi_{s,t} = h_s(\Delta \mathbf{V}_t) \end{cases} \quad (1)$$

146 For each ESM, the coefficients in the functions  $f_s$ ,  $g_s$  and  $h_s$  are estimated by minimizing  
 147 the negative log likelihood over scenarios and available ensemble members. To ensure the  
 148 convergence of the fit, the local first guess of the coefficients for the parameters is optimized  
 149 using an adapted method of moments as described in the supplementary information.

150

### 151 3.2 Spatio-temporal coherent sampling of climate extremes

152 The first step of our emulation method provides the local statistical properties of the  
 153 climate extremes and their evolution with external covariates. For approximating internal climate  
 154 variability, we aim at devising a stochastic model that produces spatially and temporally  
 155 correlated samples of TXx. To this end, we follow previous work which parameterizes internal  
 156 climate variability in annual mean temperature anomalies using a local auto-regressive processes  
 157 with spatially correlated innovations (Beusch et al., 2020). A key assumption of this approach is  
 158 that the variability is stationary in time and approximately normally distributed. This is however  
 159 not the case for residuals of the model mentioned in equation (1). Instead, we propose an  
 160 approach that exploits the model to transform TXx to a standard normal distribution using the  
 161 probability integral transform (Angus, 1994; Gneiting et al., 2007; Gudmundsson et al., 2012).  
 162 For the emulator configuration defined in Section 3.1, the GEV of TXx and its cumulative  
 163 distribution function  $\mathcal{F}_{GEV}(\Delta X_{s,t} | \Delta \mathbf{V}_t, f_s, g_s, h_s)$  are known over the full training dataset. We  
 164 define  $\mathcal{F}_{\mathcal{N}}^{-1}$  as the quantile function of the standard normal distribution. Using these two  
 165 functions, we transform  $\Delta X_{s,t}$  to a standard normally distributed transformed TXx, that we write  
 166 as  $\Phi_{s,t}$ .

$$167 \quad \Phi_{s,t} = \mathcal{F}_{\mathcal{N}}^{-1} \left( \mathcal{F}_{GEV}(\Delta X_{s,t} | \Delta \mathbf{V}_t, f_s, g_s, h_s) \right) \quad (2)$$

168 While  $\Delta X_{s,t}$  follows a non-stationary GEV distribution,  $\Phi_{s,t}$  has a normal distribution  
 169 stationary in time, thus respecting the required conditions (Humphrey and Gudmundsson, 2019;  
 170 Beusch et al., 2020). Note that no information is lost in this transformation, because the GEV  
 171 associated with  $\Phi_{s,t}$  is known at each point  $s$  and timestep  $t$ , which will be used in Section 3.3.  
 172 We train on  $\Phi_{s,t}$  a local auto-regressive process of order 1 with parameters  $\gamma_{s,0}$  and  $\gamma_{s,1}$ , with  
 173 spatially correlated innovations  $v_{s,t}$ . These innovations are sampled from a multivariate normal

174 distribution deduced from an empirically estimated and localized covariance matrix that  
 175 represents spatial dependence between points as explained in (Beusch et al., 2020).

$$176 \quad \Phi_{s,t} = \gamma_{s,0} + \gamma_{s,1}\Phi_{s,t-1} + u_{s,t} \quad (3)$$

177

### 178 3.3 Emulating spatio-temporally correlated climate extremes

179 The two steps described in section 3.1 and 3.2 form the full training of the emulator.  
 180 Here, we explain how to emulate TXx under different scenarios. Any scenario can be emulated if  
 181 it provides the covariates  $\Delta\mathbf{V}_t$  that are timeseries of anomalies in global climate variables.  
 182 Thanks to this scenario, the distribution of TXx is a direct result from equation 1.

183 Using the auto-regressive processes with spatially correlated innovations, we draw  
 184 realizations  $\Phi_{s,t,e}$  for all points  $s$ , timesteps  $t$ , and index of emulation  $e$ . These realizations are  
 185 transformations of TXx onto a standard normal distribution, and independent from the scenario  
 186 so far. Because the probability integral transformation can be reversed, we transform back the  
 187 realizations  $\Phi_{s,t,e}$  onto the distribution of TXx using its quantile function  $\mathcal{F}_{GEV}^{-1}(p|\Delta\mathbf{V}_t, f_s, g_s, h_s)$ ,  
 188  $p$  being here a probability and the cumulative distribution function of the standard normal  
 189 distribution  $\mathcal{F}_N$ , leading to the emulations of TXx written  $\Delta X_{s,t,e}$ :

$$190 \quad \Delta X_{s,t,e} = \mathcal{F}_{GEV}^{-1}(\mathcal{F}_N(\Phi_{s,t,e})|\Delta\mathbf{V}_t, f_s, g_s, h_s) \quad (4)$$

191

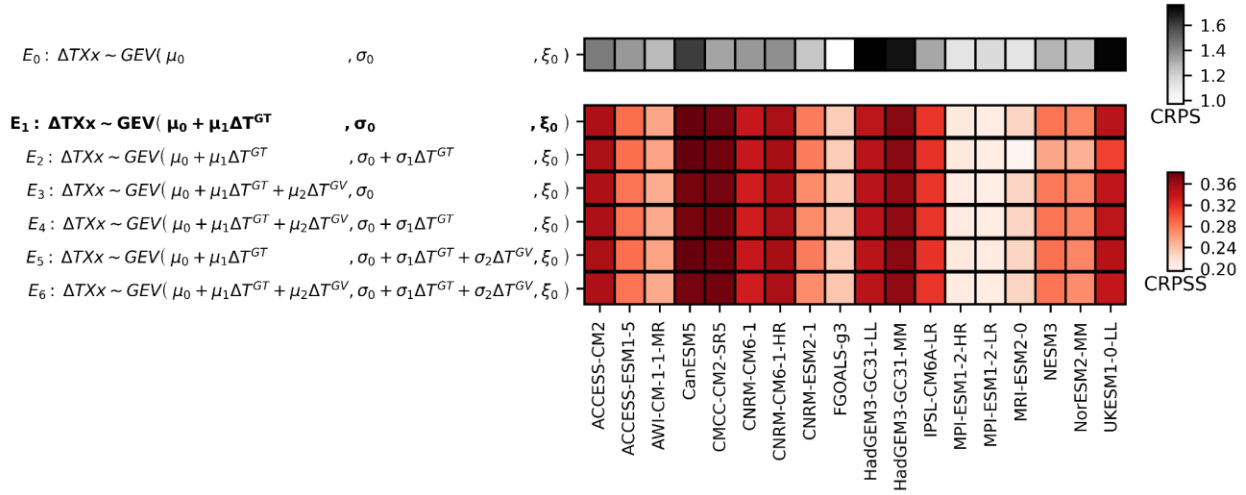
## 192 4 Emulating extreme temperatures under climate change

### 193 4.1 Evaluating and selecting emulator configurations

194 The method of Section 3 is applied and we test a set of different configurations (Figure  
 195 1), looking for a good compromise between simplicity and accuracy. For each of the 18 ESMs,  
 196 we use its historical period over 1850-2014 and all available scenarios over 2015-2100 to  
 197 calibrate the emulator configuration (Section 3.1) and the auto-regressive process with spatially-  
 198 correlated innovations (Section 3.2). We then draw 1000 realizations that we back-transform into  
 199 emulations of all available scenarios. (Section 3.3). For each ESM and emulator configuration,  
 200 we evaluate the ability of the emulations to reproduce the ESM's TXx anomaly distribution  
 201 using the Continuous Rank Probability Score (CRPS) and the CRPS Skill Score (CRPSS),  
 202 commonly used in climate sciences (Wilks, 2011; Jolliffe and Stephenson, 2012). The CRPS  
 203 measures the quadratic discrepancy between the cumulative distribution function of the  
 204 emulations to the one of the ESM. We calculate this score for each point of the sample. The  
 205 CRPSS is defined as one minus the ratio of the CRPS to another CRPS used as a reference, thus  
 206 expressing the decrease in the CRPS relative to the reference. Both scores are then averaged  
 207 globally for the sake of clarity.

208 We show a selection of emulator configurations in Figure 1, using the decomposition of  
 209 the GSAT anomaly into the global trend  $\Delta T^{GT}$  and the global variability  $\Delta T^{GV}$  (Beusch et al.,

210 2020). The global trend  $\Delta T^{GT}$  is meant to capture the signal from global warming while the  
 211 global variability  $\Delta T^{GV}$  would rather capture interannual variability processes. We use here  
 212 linear evolutions of covariates, for simplicity and given their observed linearity with global mean  
 213 temperature (Seneviratne et al., 2016; Wartenburger et al., 2017; Tebaldi et al., 2020). In Figure  
 214 1, the configurations are distinguished into two groups: the first row corresponds to a primitive  
 215 configuration, with no covariates, used for benchmarking of the second group.



216  
 217 **Figure 1.** Selection of an emulator configuration. The first row shows the CRPS (lower is better)  
 218 for the emulator configuration  $E_0$  used as a reference. On the following rows, the CRPSS (higher  
 219 is better) with reference to the emulator configuration  $E_0$  show the respective global performance  
 220 of the different emulator configurations for different ESMs.

221 On the first row of Figure 1, the emulator configuration has its GEV with constant  
 222 parameters over time, despite a changing climate. On the second row of Figure 1, the  
 223 configuration  $E_1$  has only its location covarying linearly with  $\Delta T^{GT}$ . Compared to  $E_0$ , it reduces  
 224 the CRPS on average by about 28%. The ESMs with a low CRPS in  $E_0$  (eg FGOALS-g3) have  
 225 their TXx less influenced by climate change than those with a higher CRPS such as HadGEM3-  
 226 GC31-LL, HadGEM3-GC31-MM and UKESM1-0-LL. Those ESMs with a low CRPS have a  
 227 low CRPSS as well, because the new emulator configuration brings little improvement.  
 228 However, those with a higher CRPS benefit from a stronger reduction in their CRPS by  
 229 including a dependency of the GEV to climate change.

230 On the following rows, different combinations are tried to further improve  $E_1$ . However,  
 231 these more complex models have only marginal gains, or even lead to a reduction in the  
 232 performances (e.g.  $E_2$ ). These results are confirmed by comparing the global distribution of  
 233 CRPS using Mann-Whitney U tests: adding additional terms for the emulation of TXx either  
 234 brings no significant improvement, or slightly reduces the quality of the emulations. It would  
 235 suggest that it would only overfit the data.

236 We observe that the emulator configurations  $E_2$  to  $E_6$  bring improvement only in some  
 237 regions of the Earth (not shown), while they hamper the fit in many others, which is consistent  
 238 with (Kharin and Zwiers, 2005; Kim et al., 2020). In our framework,  $E_1$  is sufficient to capture  
 239 the evolution of the distribution of TXx in a changing climate. We observe that with the

240 combination of  $\Delta T^{GT}$  and the emulated  $\Delta T^{GV}$ , the location and scale parameters vary over  
241 broader domains than those of the ESM, and the scale parameters may even become negative.  
242 Because  $\Delta T^{GV}$  can be characterized as an independent stochastic process, using it as a covariate  
243 hinders the emulation.

244 In Figures S.1 to S.7, we show other emulator configurations. We use  $\Delta H^{GT}$ , the global  
245 trend of the anomaly in HFDS, to disentangle contributions with different timescales (Geoffroy  
246 et al., 2013; King et al., 2020). It shows that  $\Delta H^{GT}$  does not bring the desired improvement: the  
247 differences in transient and equilibrium TXx appear mostly at the end of low-warming scenarios.  
248 Using the extensions of scenarios up to 2300 may help the algorithm in seizing this signal. A  
249 logistic regression is also tried on the shape parameter, to limit the range of its evolution and to  
250 account for changes in albedo, for instance due to reduction in snow cover.

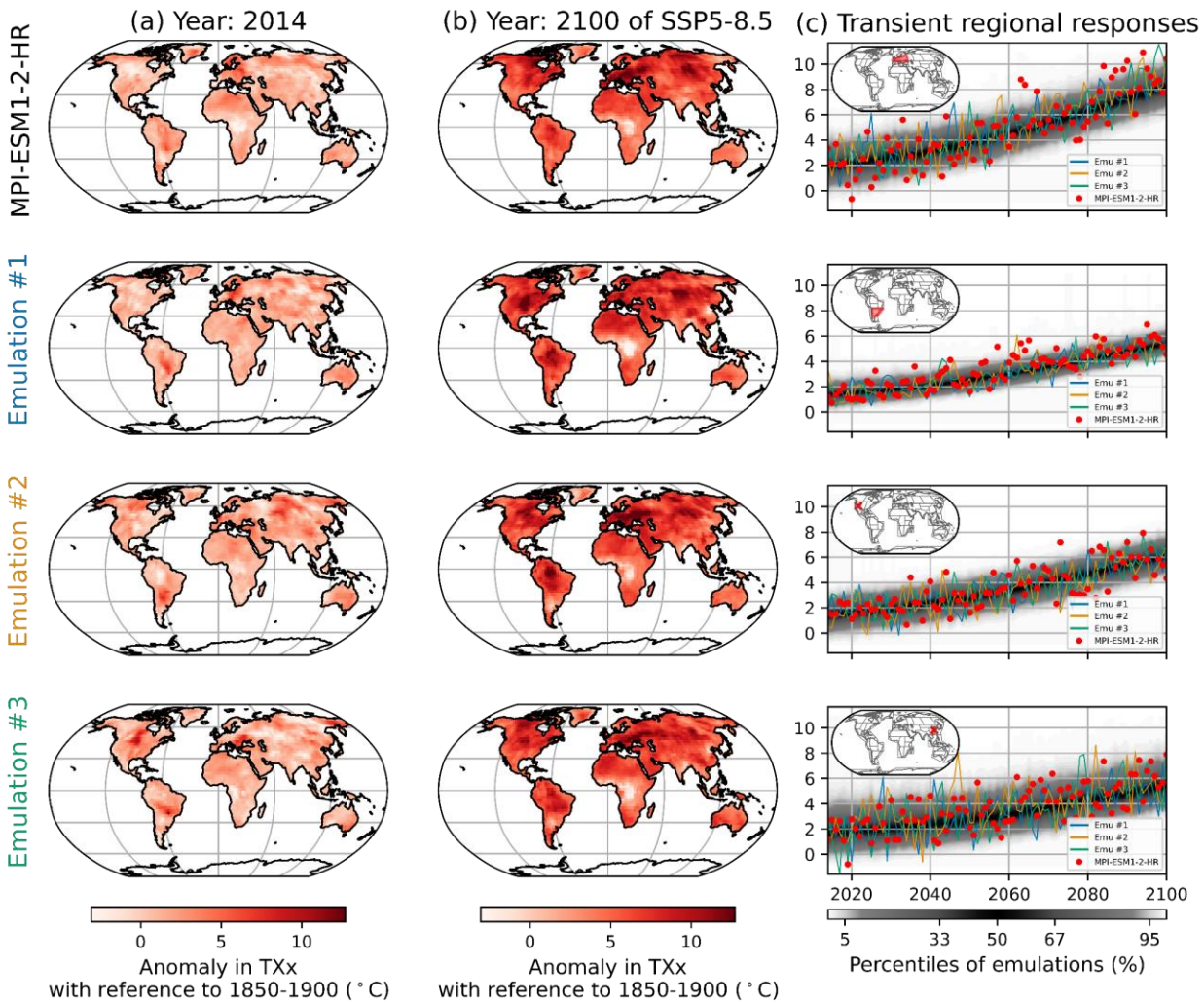
251 This analysis shows that the emulator configuration  $E_1$  provides the best compromise of  
252 simplicity and quality for emulations of TXx. The results in the rest of the paper will therefore  
253 use  $E_1$ , i.e. with the only the location parameter of the GEV varying linearly with  $\Delta T^{GT}$ .

254

## 255 4.2 Example of emulations

256 Figure 2 shows an example of our results for MPI-ESM1-2-HR, one of the 18 trained  
257 ESMs. We compare the maps of the anomaly in TXx of the ESM (topmost row) with 3 of the  
258 1000 emulations for this ESM. We show the years 2014 and 2100, the end of the historical

259 scenario and the end of SSP5-8.5 to illustrate the performance under current and high warming  
 260 conditions.



262 **Figure 2.** Example of emulations. The local anomalies in TXx are shown for MPI-ESM1-2-HR  
 263 and three emulations for the years 2014 and 2100, in columns (a) and (b), respectively. The  
 264 transient regional response from 2014 to 2100 is shown in column (c) for selected regions and  
 265 points. The 1<sup>st</sup> and 2<sup>nd</sup> rows of column (c) are respectively the regions West & Central Europe  
 266 and the South-East of South America. The 3<sup>rd</sup> and 4<sup>th</sup> rows of column (c) are two points located  
 267 in the United States and in China respectively. It features the values from MPI-ESM1-2-HR, the  
 268 same three emulations shown in maps and the density of the 1000 emulations drawn for this  
 269 emulator configuration.

270 The emulations capture the general spatial features in TXx well, be it in 2014 or in 2100,  
 271 but no exact match to the ESM simulation can be expected since they include a representation of  
 272 natural variability. For example, both the emulations and the ESM simulate the positive anomaly  
 273 over Eastern Europe and the center of South America or the lower anomaly over Central Africa.  
 274 Because each emulation includes natural variability, some features are more pronounced than

275 others, such as the high anomaly in the center of North America. The strongest differences to  
276 MPI-ESM1-2-HR are in the South-East of South America and in the center of North America.

277 To further investigate the similarities and discrepancies, we represent the transient  
278 response in two specific regions and two specific points as detailed in Figure 2. Overall, the  
279 emulations show a good agreement with the ESM. The ensemble of emulations correctly  
280 encompasses the realization by MPI-ESM1-2-HR.

281 Figures S.8 to S.25 show the same results for the 17 other ESMs employed in this study.  
282 They highlight that the emulator captures the spatial and temporal features of these models as  
283 well, even though the ESMs present different mean warming, internal variability, and spatial  
284 patterns of TXx anomalies.

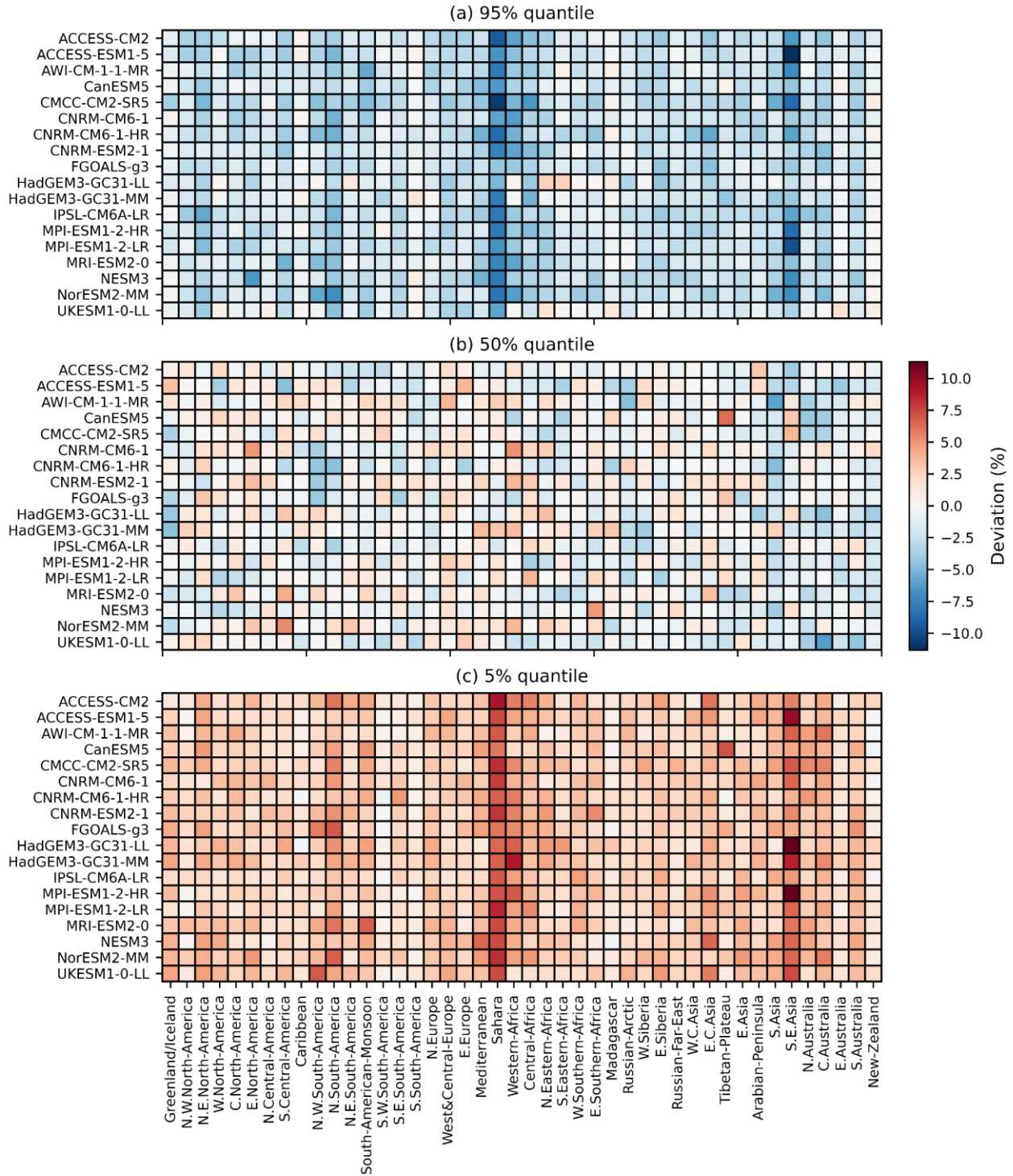
285

### 286 4.3 Evaluation of regional performance

287 We have selected the emulator configuration on the basis of its global performance in  
288 Section 4.1, and verified that the emulations are visually convincing at different spatial scales in  
289 Section 4.2. Here, we want to quantify the performance on a regional level. To do so, we  
290 compare regional percentiles of the emulations to the ESMs following the same approach as  
291 (Beusch et al., 2020). For each ESM and each emulation, the anomalies in TXx are averaged  
292 over the AR6 regions. Next, we calculate the 95%, 50% and 5% percentiles of the regional  
293 emulations. We count how often the regional values of the ESM exceed these thresholds. We  
294 determine the deviations of the ESM to the percentiles of the emulation, hence how well we  
295 reproduce the dispersion of the ESM.

296 Figure 3 shows the regional deviation in the quantiles. Panel (a) shows that the 95%  
297 quantile of the emulations is generally too low, while panel (c) shows that the 5% quantile of the  
298 emulations is mostly too high. This means that the emulation is underdispersive, a feature  
299 expected for emulations (Beusch et al., 2020). The performance of the emulator is lowest in  
300 South-East Asia and in the Sahara, but overall the performance remains good: the regional  
301 deviations are below 5% in most of the cases (for 93%, 99% and 92% of the model-region  
302 combinations for the quantiles 95%, 50% and 5%, respectively). The average of the regional  
303 deviations across regions and ESMs is -2.4%, -0.3% and 2.9%.

304



305

306 **Figure 3.** Regional deviations of ESMs from the 5%, 50%, 95% quantiles of the emulations,  
 307 respectively in panels (a), (b) and (c). Red (blue) indicates that the quantile of the emulations is  
 308 higher (lower) than the one of ESM, because the ESM is more frequently below (above) the  
 309 quantile than expected.

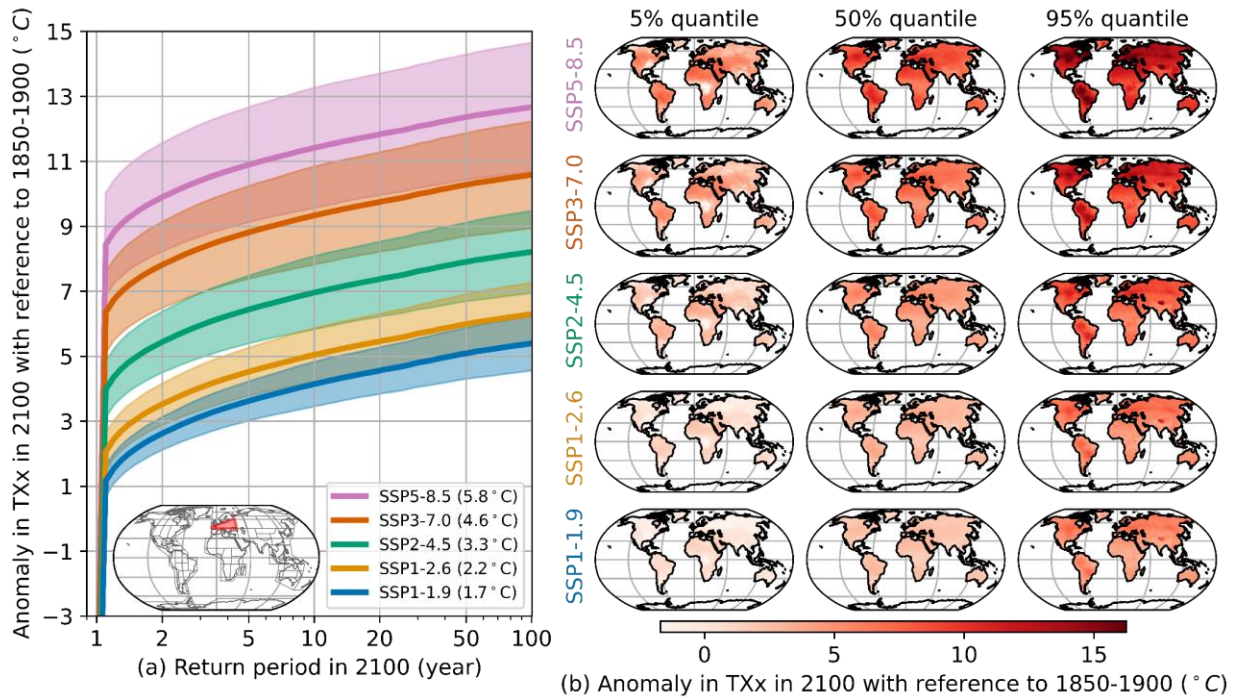
310

## 311 4.4 Example application

312 In Sections 4.1 to 4.3, we evaluate the performance of the emulator using training data.  
313 However, this method is not only meant to reproduce training data, but also to emulate other  
314 scenarios. For instance, some ESMs run only a subset of the scenarios SSP1-1.9, SS1-2.6, SSP2-  
315 4.5, SSP3-7.0 and SSP5-8.5, which hinders the evaluation of a distribution of anomalies in TXx  
316 based on all ESMs. Here, for each ESM, we use the emulator trained on available scenarios from  
317 Sections 4.2 to 4.3 to calculate all these SSPs.

318 In the selected configuration, MESMER-X can emulate scenarios if timeseries of the  
319 smoothed anomaly in GSAT ( $\Delta T^{GT}$ ) are provided. For each of the scenarios (Section 2), we  
320 average  $\Delta T^{GT}$  over all ESMs that have run the scenario. These averaged  $\Delta T^{GT}$  are used as  
321 common drivers to create emulations for all ESMs for every scenario. For each of the 18 ESMs,  
322 we calculate an ensemble of 1000 realizations which combines two sources of dispersion: the  
323 local variability in TXx modeled by the ESM and the uncertainty in this modeling by ESMs, also  
324 termed “regional climate sensitivity” (Seneviratne and Hauser, 2020). Yet, it does not encompass  
325 the global uncertainty due to the different global climate sensitivities of the ESMs. Additionally,  
326 we are not weighting ESMs according to their performances nor accounting for ESM-  
327 interdependencies (Abramowitz et al., 2019; Brunner et al., 2020b). Here, we solely aim to show the  
328 capacity of this emulator by synthesizing differences in the modeling of TXx in the ESMs. Using  
329 the emulations, we calculate the distributions of the anomaly in TXx for any point in space and  
330 time, as illustrated in the right panel of Figure 4. From these emulations, we deduce the return  
331 periods in 2100 for each ESM and scenario. Then we deduce the mean and standard deviation of

332 these return periods, corresponding to the uncertainty induced by the different ESMS' different  
 333 representation of natural variability, as shown in left panel of Figure 4.



334

335 **Figure 4.** Illustration of the ensemble formed by 1000 emulations of the 18 trained ESMS,  
 336 applied over common scenarios. The return periods in 2100 in West & Central Europe of each  
 337 ESMS are shown in panel (a) through their mean and one standard deviation range. In the legend,  
 338 the anomaly in GSAT in 2100 of each scenario is provided. Panel (b) shows the local 5%, 50%  
 339 and 95% quantiles in 2100, all ESMS being pooled together. Each row corresponds to a different  
 340 scenario.

341 In the left panel of Figure 4, we notice that in West & Central Europe, an anomaly of 5°C  
 342 would happen about once in 40 years in 2100 under SSP1-1.9, but every 10 years under SSP1-  
 343 2.6 and every 1 or 2 years under SSP2-4.5. This result is consistent with how climate extremes  
 344 are projected for 1.5°C (Seneviratne et al., 2018) and the change from 1.5°C to 2°C (Hoegh-  
 345 Guldberg et al., 2018).

346 In the right panel of Figure 4, we show the maps in 2100 for selected quantiles. Here, all  
 347 emulations and ESMS are pooled together, which implies that both the natural local variability in  
 348 TXx and the uncertainty in this modeling by ESMS contribute to this range. For the median, the  
 349 regions with the highest anomalies of TXx are Central North America, Central South America  
 350 and the Mediterranean region. Those with the lowest anomalies are Greenland, South Asia and  
 351 Central Africa. These results are even more distinct when considering the 95% quantile. The  
 352 95% quantile of SSP1-1.9 seems overall only slightly higher than the 5% quantile of SSP5-8.5.

353 Broadly speaking, it would suggest that anomalies in TXx that had only 5% of chances to occur  
354 or be exceeded in SSP1-1.9 in 2100, would have their probability increase to 95% in SSP5-8.5.

355

## 356 **5 Discussion and conclusions**

357 This paper has introduced a method for the emulation of climate extremes under climate  
358 change, used to extend the MESMER emulator (Beusch et al., 2020) to MESMER-X. This  
359 method does not only reproduce the mean evolution of climate extremes but also their  
360 distribution. Besides, it accounts for their spatial and temporal features.

361 Fits of non-stationnary GEV for TXx have already been performed using different  
362 covariates on the location (Zwiers et al., 2011; Hauser et al., 2016; Wehner et al., 2020; Wehner,  
363 2020). Here, we leverage this approach to model the distribution of TXx at each point  
364 conditional on global covariates. The proposed method is improved in its greater versatility in  
365 the use of covariates and in its sampling of stochastic realizations of timeseries fields. We show  
366 that the emulator mimics well the local annual maximum temperature of the ESMs, with an  
367 underdispersion below 5% for most regions and ESMs.

368 This method is designed to be directly applied to other indicators of climate extremes, as  
369 long as their distribution can be parametrized by a GEV. Moreover, the framework can be easily  
370 adapted to different distributions which be more appropriate for other indicators, such as a  
371 Poisson distribution for counting extreme events (Wilks, 2011) or a generalized Pareto  
372 distribution for climate extremes based on peak-over-threshold exceedances (Coles, 2001;  
373 Naveau et al., 2005). The parameters of these distributions may vary with any combination of  
374 global drivers to improve the quality of the emulator configuration.

375 Similar to MESMER (Beusch et al., 2022a; Beusch et al., 2022b), MESMER-X could be  
376 coupled to a SCM in future work to gain the ability to transform any emission scenario into local  
377 annual climate extremes in a fast and probabilistic way. Such an emulator chain could be used to  
378 provide detailed climate information into integrated assessment models, for instance to  
379 assess how climate extremes affect different transformation pathways.

380 (All figures and tables should be cited in order. For initial submission, please embed figures, tables, and their  
381 captions within the main text near where they are cited. At revision, figures should be uploaded separately, as we  
382 need separate files for production. Tables and all captions should be moved to the end of the file.)

383

## 384 **Acknowledgments**

385 We acknowledge the World Climate Research Program for the coordination and promotion of  
386 CMIP6. We thank the climate modeling groups for producing their model outputs and making  
387 them available. We acknowledge the Earth System Grid Federation for archiving the data and  
388 providing access. We thank Urs Beyerle for the download and curation of CMIP6 data, and  
389 Lukas Brunner for the processing into the CMIP6-ng archive. We acknowledge the European  
390 Research Council (ERC) for the ERC Proof Of Concept Grant MESMER-X (Grant Agreement  
391 ID 964013) that funded this work.

392

393

394 **Open Research**

395 Data from CMIP6 is available at <https://esgf-node.llnl.gov/projects/esgf-llnl/> (last access: 3 April  
396 2022). Code from MESMER is available at <https://github.com/MESMER-group/mesmer>.

397

398

399 **References**

- 400 Abramowitz, G., Herger, N., Gutmann, E., Hammerling, D., Knutti, R., Leduc, M., Lorenz, R., Pincus, R., and  
401 Schmidt, G. A.: ESD Reviews: Model dependence in multi-model climate ensembles: weighting, sub-selection and  
402 out-of-sample testing, *Earth Syst. Dynam.*, 10, 91-105, 10.5194/esd-10-91-2019, 2019.
- 403 Alexeeff, S. E., Nychka, D., Sain, S. R., and Tebaldi, C.: Emulating mean patterns and variability of temperature  
404 across and within scenarios in anthropogenic climate change experiments, *Climatic Change*, 146, 319-333,  
405 10.1007/s10584-016-1809-8, 2018.
- 406 Angus, J. E.: The probability integral transform and related results, *SIAM review*, 36, 652-654, 1994.
- 407 AON: Weather, climate & catastrophe insight, 2020 Annual Report, 2021.
- 408 Beusch, L., Gudmundsson, L., and Seneviratne, S. I.: Emulating Earth system model temperatures with MESMER:  
409 from global mean temperature trajectories to grid-point-level realizations on land, *Earth Syst. Dynam.*, 11, 139-159,  
410 10.5194/esd-11-139-2020, 2020.
- 411 Beusch, L., Nauels, A., Gudmundsson, L., Gütschow, J., Schleussner, C.-F., and Seneviratne, S. I.: Responsibility of  
412 major emitters for country-level warming and extreme hot years, *Communications Earth & Environment*, 3, 7,  
413 10.1038/s43247-021-00320-6, 2022a.
- 414 Beusch, L., Nicholls, Z., Gudmundsson, L., Hauser, M., Meinshausen, M., and Seneviratne, S. I.: From emission  
415 scenarios to spatially resolved projections with a chain of computationally efficient emulators: coupling of  
416 MAGICC (v7.5.1) and MESMER (v0.8.3), *Geosci. Model Dev.*, 15, 2085-2103, 10.5194/gmd-15-2085-2022,  
417 2022b.
- 418 Brunner, L., Hauser, M., Lorenz, R., and Beyerle, U.: The ETH Zurich CMIP6 next generation archive: technical  
419 documentation (v1.0-final), Zenodo, <https://doi.org/10.5281/zenodo.3734128>, 2020a.
- 420 Brunner, L., Pendergrass, A. G., Lehner, F., Merrifield, A. L., Lorenz, R., and Knutti, R.: Reduced global warming  
421 from CMIP6 projections when weighting models by performance and independence, *Earth Syst. Dynam. Discuss.*,  
422 2020, 1-23, 10.5194/esd-2020-23, 2020b.
- 423 Castruccio, S., McInerney, D. J., Stein, M. L., Liu Crouch, F., Jacob, R. L., and Moyer, E. J.: Statistical Emulation  
424 of Climate Model Projections Based on Precomputed GCM Runs, *Journal of Climate*, 27, 1829-1844,  
425 10.1175/JCLI-D-13-00099.1, 2014.
- 426 Coles, S.: An introduction to statistical modeling of extreme values, Springer, London; New York 2001.
- 427 Collins, M., Knutti, R., Arblaster, J., Dufresne, J.-L., Fichet, T., Friedlingstein, P., Gao, X., Gutowski, W. J.,  
428 Johns, T., Krinner, G., Shongwe, M., Tebaldi, C., Weaver, A. J., and Wehner, M.: Long-term Climate Change:  
429 Projections, Commitments and Irreversibility, in: *Climate Change 2013: The Physical Science Basis. Contribution*  
430 *of Working Group I to the Fifth Assessment Report of the Intergovernmental Panel on Climate Change*, edited by:  
431 Stocker, T. F., Qin, D., Plattner, G. K., Tignor, M., Allen, S. K., Boschung, J., Nauels, A., Xia, Y., Bex, V., and  
432 Midgley, P. M., Cambridge University Press, Cambridge, United Kingdom and New York, NY, USA, 1029-1136,  
433 2013.
- 434 Eyring, V., Bony, S., Meehl, G. A., Senior, C. A., Stevens, B., Stouffer, R. J., and Taylor, K. E.: Overview of the  
435 Coupled Model Intercomparison Project Phase 6 (CMIP6) experimental design and organization, *Geoscientific*  
436 *Model Development*, 9, 1937-1958, 2016.
- 437 Flato, G., Marotzke, J., Abiodun, B., Braconnot, P., Chou, S. C., Collins, W., Cox, P., Driouech, F., Emori, S.,  
438 Eyring, V., Forest, C., Gleckler, P., Guilyardi, E., Jakob, C., Kattsov, V., Reason, C., and Rummukainen, M.:

439 Evaluation of Climate Models, in: Climate Change 2013: The Physical Science Basis. Contribution of Working  
440 Group I to the Fifth Assessment Report of the Intergovernmental Panel on Climate Change, edited by: Stocker, T.  
441 F., Qin, D., Plattner, G. K., Tignor, M., Allen, S. K., Boschung, J., Nauels, A., Xia, Y., Bex, V., and Midgley, P. M.,  
442 Cambridge University Press, Cambridge, United Kingdom and New York, NY, USA, 741-866, 2013.

443 Fordham, D. A., Wigley, T. M. L., Watts, M. J., and Brook, B. W.: Strengthening forecasts of climate change  
444 impacts with multi-model ensemble averaged projections using MAGICC/SCENGEN 5.3, *Ecography*, 35, 4-8,  
445 <https://doi.org/10.1111/j.1600-0587.2011.07398.x>, 2012.

446 Geoffroy, O., Saint-Martin, D., Bellon, G., Voltaire, A., Olivie, D. J. L., and Tyteca, S.: Transient Climate  
447 Response in a Two-Layer Energy-Balance Model. Part II: Representation of the Efficacy of Deep-Ocean Heat  
448 Uptake and Validation for CMIP5 AOGCMs, *Journal of Climate*, 26, 1859-1876, 10.1175/JCLI-D-12-00196.1,  
449 2013.

450 Gneiting, T., Balabdaoui, F., and Raftery, A. E.: Probabilistic forecasts, calibration and sharpness, *Journal of the*  
451 *Royal Statistical Society: Series B (Statistical Methodology)*, 69, 243-268, [https://doi.org/10.1111/j.1467-](https://doi.org/10.1111/j.1467-9868.2007.00587.x)  
452 [9868.2007.00587.x](https://doi.org/10.1111/j.1467-9868.2007.00587.x), 2007.

453 Gudmundsson, L., Bremnes, J. B., Haugen, J. E., and Engen-Skaugen, T.: Technical Note: Downscaling RCM  
454 precipitation to the station scale using statistical transformations &ndash; a comparison of methods, *Hydrol. Earth*  
455 *Syst. Sci.*, 16, 3383-3390, 10.5194/hess-16-3383-2012, 2012.

456 Hasegawa, T., Sakurai, G., Fujimori, S., Takahashi, K., Hijioka, Y., and Masui, T.: Extreme climate events increase  
457 risk of global food insecurity and adaptation needs, *Nature Food*, 2, 587-595, 10.1038/s43016-021-00335-4, 2021.

458 Hauser, M., Orth, R., and Seneviratne, S. I.: Role of soil moisture versus recent climate change for the 2010 heat  
459 wave in western Russia, *Geophysical Research Letters*, 43, 2819-2826, <https://doi.org/10.1002/2016GL068036>,  
460 2016.

461 Herger, N., Sanderson, B. M., and Knutti, R.: Improved pattern scaling approaches for the use in climate impact  
462 studies, *Geophysical Research Letters*, 42, 3486-3494, <https://doi.org/10.1002/2015GL063569>, 2015.

463 Hoegh-Guldberg, O., Jacob, D., Taylor, M., Bindi, M., Brown, S., Camilloni, I., Diedhiou, A., Djalante, R., Ebi, K.,  
464 Engelbrecht, F., Guiot, J., Hijioka, Y., Mehrotra, S., Payne, A., Seneviratne, S. I., Thomas, A., Warren, R., and  
465 Zhou, G.: Impacts of 1.5°C global warming on natural and human systems, in: Global warming of 1.5°C. An IPCC  
466 Special Report on the impacts of global warming of 1.5°C above pre-industrial levels and related global greenhouse  
467 gas emission pathways, in the context of strengthening the global response to the threat of climate change,  
468 sustainable development, and efforts to eradicate poverty, edited by: Masson-Delmotte, V., Zhai, P., Pörtner, H. O.,  
469 Roberts, D., Skea, J., Shukla, P. R., Pirani, A., Moufouma-Okia, W., Péan, C., Pidcock, R., Connors, S., Matthews,  
470 J. B. R., Chen, Y., Zhou, X., Gomis, M. I., Lonnoy, E., Maycock, T., Tignor, M., and Waterfield, T., In Press,  
471 <https://www.ipcc.ch/sr15/download/>, 2018.

472 Holden, P. B., Edwards, N. R., Garthwaite, P. H., Fraedrich, K., Lunkeit, F., Kirk, E., Labriet, M., Kanudia, A., and  
473 Babonneau, F.: PLASIM-ENTSem v1.0: a spatio-temporal emulator of future climate change for impacts  
474 assessment, *Geosci. Model Dev.*, 7, 433-451, 10.5194/gmd-7-433-2014, 2014.

475 Huang, W. K., Stein, M. L., McInerney, D. J., Sun, S., and Moyer, E. J.: Estimating changes in temperature  
476 extremes from millennial-scale climate simulations using generalized extreme value (GEV) distributions, *Adv. Stat.*  
477 *Clim. Meteorol. Oceanogr.*, 2, 79-103, 10.5194/ascmo-2-79-2016, 2016.

478 Humphrey, V. and Gudmundsson, L.: GRACE-REC: a reconstruction of climate-driven water storage changes over  
479 the last century, *Earth Syst. Sci. Data*, 11, 1153-1170, 10.5194/essd-11-1153-2019, 2019.

480 IPCC, Field, C. B., Barros, V. R., Dokken, D. J., Mach, K. J., Mastrandrea, M. D., Bilir, T. E., Chatterjee, M., Ebi,  
481 K. L., Estrada, Y. O., Genova, R. C., Girma, B., Kissel, E. S., Levy, A. N., MacCracken, S., Mastrandrea, P. R.,  
482 White, L. L., and (eds.) (Eds.): Climate Change 2014: Impacts, Adaptation, and Vulnerability. Part A: Global and  
483 Sectoral Aspects. Contribution of Working Group II to the Fifth Assessment Report of the Intergovernmental Panel  
484 on Climate  
485 Change, Cambridge University Press, 2014.

486 IPCC: Global warming of 1.5C. An IPCC Special Report on the impacts of global warming of 1.5C above  
487 pre-industrial levels and related global greenhouse gas emission pathways, in the context of strengthening the  
488 global response to the threat of climate change, sustainable development, and efforts to eradicate poverty, In  
489 Press2018.

490 IPCC, Masson-Delmotte, V., Zhai, P., Pirani, A., Connors, S. L., Péan, C., Berger, S., Caud, N., Chen, Y., Goldfarb,  
491 L., Gomis, M. I., Huang, M., Leitzell, K., Lonnoy, E., Matthews, J. B. R., Maycock, T. K., Waterfield, T., Yelekçi,  
492 O., Yu, R., and Zhou, B. (Eds.): Climate Change 2021: The Physical Science Basis. Contribution of Working Group  
493 I to the Sixth Assessment Report of the Intergovernmental Panel on Climate Change, Cambridge University  
494 Press2021.

495 Iturbide, M., Gutiérrez, J. M., Alves, L. M., Bedia, J., Cerezo-Mota, R., Gimenez, E., Cofiño, A. S., Di Luca, A.,  
496 Faria, S. H., Gorodetskaya, I. V., Hauser, M., Herrera, S., Hennessy, K., Hewitt, H. T., Jones, R. G., Krakovska, S.,  
497 Manzanas, R., Martínez-Castro, D., Narisma, G. T., Nurhati, I. S., Pinto, I., Seneviratne, S. I., van den Hurk, B., and  
498 Vera, C. S.: An update of IPCC climate reference regions for subcontinental analysis of climate model data:  
499 definition and aggregated datasets, *Earth Syst. Sci. Data*, 12, 2959-2970, 10.5194/essd-12-2959-2020, 2020.  
500 Jolliffe, I. T. and Stephenson, D. B.: *Forecast verification: a practitioner's guide in atmospheric science*, John Wiley  
501 & Sons 2012.

502 Kharin, V. V. and Zwiers, F. W.: Estimating Extremes in Transient Climate Change Simulations, *Journal of*  
503 *Climate*, 18, 1156-1173, 10.1175/JCLI3320.1, 2005.

504 Kim, Y.-H., Min, S.-K., Zhang, X., Sillmann, J., and Sandstad, M.: Evaluation of the CMIP6 multi-model ensemble  
505 for climate extreme indices, *Weather and Climate Extremes*, 29, 100269,  
506 <https://doi.org/10.1016/j.wace.2020.100269>, 2020.

507 King, A. D., Lane, T. P., Henley, B. J., and Brown, J. R.: Global and regional impacts differ between transient and  
508 equilibrium warmer worlds, *Nature Climate Change*, 10, 42-47, 10.1038/s41558-019-0658-7, 2020.

509 Lee, J. Y., Marotzke, J., Bala, G., Cao, L., Corti, S., Dunne, J. P., Engelbrecht, F., Fischer, E., Fyfe, J. C., Jones, C.,  
510 Maycock, A., Mutemi, J., Ndiaye, O., Panickal, S., and Zhou, T.: Future Global Climate: Scenario Based Projections  
511 and Near-Term Information, in: *Climate Change 2021: The Physical Science Basis. Contribution of Working Group*  
512 *I to the Sixth Assessment Report of the Intergovernmental Panel on Climate Change*, edited by: Masson-Delmotte,  
513 V., Zhai, P., Pirani, A., Connors, S. L., Péan, C., Berger, S., Caud, N., Chen, Y., Goldfarb, L., Gomis, M. I., Huang,  
514 M., Leitzell, K., Lonnoy, E., Matthews, J. B. R., Maycock, T. K., Waterfield, T., Yelekçi, O., Yu, R., and Zhou, B.,  
515 Cambridge University Press, 2021.

516 Link, R., Snyder, A., Lynch, C., Hartin, C., Kravitz, B., and Bond-Lamberty, B.: Fldgen v1.0: an emulator with  
517 internal variability and space-time correlation for Earth system models, *Geosci. Model Dev.*, 12, 1477-1489,  
518 10.5194/gmd-12-1477-2019, 2019.

519 Lynch, C., Hartin, C., Bond-Lamberty, B., and Kravitz, B.: An open-Access CMIP5 pattern library for temperature  
520 and precipitation: Description and methodology, *Earth System Science Data*, 9, 281-292, 2017.

521 McKinnon, K. A., Poppick, A., Dunn-Sigouin, E., and Deser, C.: An "Observational Large Ensemble" to Compare  
522 Observed and Modeled Temperature Trend Uncertainty due to Internal Variability, *Journal of Climate*, 30, 7585-  
523 7598, 10.1175/JCLI-D-16-0905.1, 2017.

524 Meinshausen, M., Nicholls, Z. R. J., Lewis, J., Gidden, M. J., Vogel, E., Freund, M., Beyerle, U., Gessner, C.,  
525 Nauels, A., Bauer, N., Canadell, J. G., Daniel, J. S., John, A., Krummel, P. B., Luderer, G., Meinshausen, N.,  
526 Montzka, S. A., Rayner, P. J., Reimann, S., Smith, S. J., van den Berg, M., Velders, G. J. M., Vollmer, M. K., and  
527 Wang, R. H. J.: The shared socio-economic pathway (SSP) greenhouse gas concentrations and their extensions to  
528 2500, *Geosci. Model Dev.*, 13, 3571-3605, 10.5194/gmd-13-3571-2020, 2020.

529 Meinshausen, M., Vogel, E., Nauels, A., Lorbacher, K., Meinshausen, N., Etheridge, D. M., Fraser, P. J., Montzka,  
530 S. A., Rayner, P. J., Trudinger, C. M., Krummel, P. B., Beyerle, U., Canadell, J. G., Daniel, J. S., Enting, I. G., Law,  
531 R. M., Lunder, C. R., O'Doherty, S., Prinn, R. G., Reimann, S., Rubino, M., Velders, G. J. M., Vollmer, M. K.,  
532 Wang, R. H. J., and Weiss, R.: Historical greenhouse gas concentrations for climate modelling (CMIP6),  
533 *Geoscientific Model Development*, 10, 2057-2116, 2017.

534 Mitchell, T. D.: Pattern Scaling: An Examination of the Accuracy of the Technique for Describing Future Climates,  
535 *Climatic Change*, 60, 217-242, 10.1023/A:1026035305597, 2003.

536 Nath, S., Lejeune, Q., Beusch, L., Schleussner, C. F., and Seneviratne, S. I.: MESMER-M: an Earth System Model  
537 emulator for spatially resolved monthly temperatures, *Earth Syst. Dynam. Discuss.*, 2021, 1-38, 10.5194/esd-2021-  
538 59, 2021.

539 Naveau, P., Nogaj, M., Ammann, C., Yiou, P., Cooley, D., and Jomelli, V.: Statistical methods for the analysis of  
540 climate extremes, *Comptes Rendus Geoscience*, 337, 1013-1022, <https://doi.org/10.1016/j.crte.2005.04.015>, 2005.

541 Nicholls, Z., Meinshausen, M., Lewis, J., Corradi, M. R., Dorheim, K., Gasser, T., Gieseke, R., Hope, A. P., Leach,  
542 N. J., McBride, L. A., Quilcaille, Y., Rogelj, J., Salawitch, R. J., Samset, B. H., Sandstad, M., Shiklomanov, A.,  
543 Skeie, R. B., Smith, C. J., Smith, S. J., Su, X., Tsutsui, J., Vega-Westhoff, B., and Woodard, D. L.: Reduced  
544 Complexity Model Intercomparison Project Phase 2: Synthesising Earth system knowledge for probabilistic climate  
545 projections, *Earth's Future*, n/a, e2020EF001900, <https://doi.org/10.1029/2020EF001900>, 2021.

546 Nicholls, Z. R. J., Meinshausen, M., Lewis, J., Gieseke, R., Dommenges, D., Dorheim, K., Fan, C. S., Fuglestad, J.  
547 S., Gasser, T., Golüke, U., Goodwin, P., Kriegler, E., Leach, N. J., Marchegiani, D., Quilcaille, Y., Samset, B. H.,  
548 Sandstad, M., Shiklomanov, A. N., Skeie, R. B., Smith, C. J., Tanaka, K., Tsutsui, J., and Xie, Z.: Reduced  
549 complexity model intercomparison project phase 1: Protocol, results and initial observations, *Geosci. Model Dev.*  
550 *Discuss.*, 2020, 1-33, 10.5194/gmd-2019-375, 2020.

551 O'Neill, B. C., Tebaldi, C., Van Vuuren, D. P., Eyring, V., Friedlingstein, P., Hurtt, G., Knutti, R., Kriegler, E.,  
552 Lamarque, J. F., Lowe, J., Meehl, G. A., Moss, R., Riahi, K., and Sanderson, B. M.: The Scenario Model  
553 Intercomparison Project (ScenarioMIP) for CMIP6, *Geoscientific Model Development*, 9, 3461-3482, 2016.  
554 Perera, A. T. D., Nik, V. M., Chen, D., Scartezzini, J.-L., and Hong, T.: Quantifying the impacts of climate change  
555 and extreme climate events on energy systems, *Nature Energy*, 5, 150-159, 10.1038/s41560-020-0558-0, 2020.  
556 Raymond, C., Horton, R. M., Zscheischler, J., Martius, O., AghaKouchak, A., Balch, J., Bowen, S. G., Camargo, S.  
557 J., Hess, J., Kornhuber, K., Oppenheimer, M., Ruane, A. C., Wahl, T., and White, K.: Understanding and managing  
558 connected extreme events, *Nature Climate Change*, 10, 611-621, 10.1038/s41558-020-0790-4, 2020.  
559 Rosenzweig, C., Arnell, N. W., Ebi, K. L., Lotze-Campen, H., Raes, F., Rapley, C., Smith, M. S., Cramer, W.,  
560 Frieler, K., Reyer, C. P. O., Schewe, J., van Vuuren, D., and Warszawski, L.: Assessing inter-sectoral climate  
561 change risks: the role of ISIMIP, *Environmental Research Letters*, 12, 010301, 10.1088/1748-9326/12/1/010301,  
562 2017.  
563 Schaeffer, R., Szklo, A. S., Pereira de Lucena, A. F., Moreira Cesar Borba, B. S., Pupo Nogueira, L. P., Fleming, F.  
564 P., Troccoli, A., Harrison, M., and Boulahya, M. S.: Energy sector vulnerability to climate change: A review,  
565 *Energy*, 38, 1-12, <https://doi.org/10.1016/j.energy.2011.11.056>, 2012.  
566 Seneviratne, S. I. and Hauser, M.: Regional Climate Sensitivity of Climate Extremes in CMIP6 Versus CMIP5  
567 Multimodel Ensembles, *Earth's Future*, 8, e2019EF001474, <https://doi.org/10.1029/2019EF001474>, 2020.  
568 Seneviratne, S. I., Donat, M. G., Pitman, A. J., Knutti, R., and Wilby, R. L.: Allowable CO2 emissions based on  
569 regional and impact-related climate targets, *Nature*, 529, 477-483, 10.1038/nature16542, 2016.  
570 Seneviratne, S. I., Zhang, X., Adnan, M., Badi, W., Dereczynski, C., Di Luca, A., Ghosh, S., Iskandar, I., Kossin, J.,  
571 Lewis, S., Otto, F., Pinto, I., Satoh, M., Vicente-Serrano, S. M., Wehner, M., and Zhou, B.: Weather and Climate  
572 Extreme Events in a Changing Climate, in: *Climate Change 2021: The Physical Science Basis. Contribution of*  
573 *Working Group I to the Sixth Assessment Report of the Intergovernmental Panel on Climate Change*, edited by:  
574 Masson-Delmotte, V., Zhai, P., Pirani, A., Connors, S. L., Péan, C., Berger, S., Caud, N., Chen, Y., Goldfarb, L.,  
575 Gomis, M. I., Huang, M., Leitzell, K., Lonnoy, E., Matthews, J. B. R., Maycock, T. K., Waterfield, T., Yelekçi, O.,  
576 Yu, R., and Zhou, B. e., Cambridge University Press, 2021.  
577 Seneviratne, S. I., Wartenburger, R., Guillod, B. P., Hirsch, A. L., Vogel, M. M., Brovkin, V., van Vuuren, D. P.,  
578 Schaller, N., Boysen, L., Calvin, K. V., Doelman, J., Greve, P., Havlik, P., Humpenöder, F., Krisztin, T., Mitchell,  
579 D., Popp, A., Riahi, K., Rogelj, J., Schleussner, C.-F., Sillmann, J., and Stehfest, E.: Climate extremes, land-climate  
580 feedbacks and land-use forcing at 1.5°C, *Philosophical Transactions of the Royal Society A: Mathematical, Physical*  
581 *and Engineering Sciences*, 376, 20160450, 10.1098/rsta.2016.0450, 2018.  
582 Sivakumar, M. V., Motha, R. P., and Das, H. P.: *Natural disaster and extreme events in agriculture*, Springer2005.  
583 Storch, H. v. and Zwiers, F. W.: *Statistical Analysis in Climate Research*, Cambridge University Press, Cambridge,  
584 DOI: 10.1017/CBO9780511612336, 1999.  
585 Tebaldi, C. and Arblaster, J. M.: Pattern scaling: Its strengths and limitations, and an update on the latest model  
586 simulations, *Climatic Change*, 122, 459-471, 10.1007/s10584-013-1032-9, 2014.  
587 Tebaldi, C. and Knutti, R.: Evaluating the accuracy of climate change pattern emulation for low warming targets,  
588 *Environmental Research Letters*, 13, 055006, 10.1088/1748-9326/aabef2, 2018.  
589 Tebaldi, C., Armbruster, A., Engler, H. P., and Link, R.: Emulating climate extreme indices, *Environmental*  
590 *Research Letters*, 15, 074006, 10.1088/1748-9326/ab8332, 2020.  
591 Vogel, E., Donat, M. G., Alexander, L. V., Meinshausen, M., Ray, D. K., Karoly, D., Meinshausen, N., and Frieler,  
592 K.: The effects of climate extremes on global agricultural yields, *Environmental Research Letters*, 14, 054010,  
593 10.1088/1748-9326/ab154b, 2019.  
594 Wartenburger, R., Hirschi, M., Donat, M. G., Greve, P., Pitman, A. J., and Seneviratne, S. I.: Changes in regional  
595 climate extremes as a function of global mean temperature: an interactive plotting framework, *Geoscientific Model*  
596 *Development Discussions*, 1-30, 2017.  
597 Wehner, M., Gleckler, P., and Lee, J.: Characterization of long period return values of extreme daily temperature  
598 and precipitation in the CMIP6 models: Part 1, model evaluation, *Weather and Climate Extremes*, 30, 100283,  
599 <https://doi.org/10.1016/j.wace.2020.100283>, 2020.  
600 Wehner, M. F.: Characterization of long period return values of extreme daily temperature and precipitation in the  
601 CMIP6 models: Part 2, projections of future change, *Weather and Climate Extremes*, 30, 100284,  
602 <https://doi.org/10.1016/j.wace.2020.100284>, 2020.  
603 Wilks, D. S.: *Statistical methods in the atmospheric sciences*, 2011.  
604 Zwiers, F. W., Zhang, X., and Feng, Y.: Anthropogenic Influence on Long Return Period Daily Temperature  
605 Extremes at Regional Scales, *Journal of Climate*, 24, 881-892, 10.1175/2010JCLI3908.1, 2011.  
606